Green Chemistry

PAPER

View Article Online
View Journal | View Issue

Check for updates

Cite this: *Green Chem.*, 2025, **27**, 12830

One-pot depolymerization–repolymerization of PET waste into sustainable photocurable liquid copolyesters for high-performance additive manufacturing

Rosario Carmenini, [a] Alberto Sanz de León, [b] Tiziana Benelli, [a,c] Loris Giorgini, [a,c] Mauro Comes Franchini, [a] Sergio I. Molina[b] and Mirko Maturi *[b]

In this work, we present a sustainable one-pot two-step approach for the depolymerization and repolymerization of post-consumer poly(ethylene terephthalate) (PET) into high-performance photocurable liquid polyesters suitable for vat photopolymerization (VP) additive manufacturing. By coupling PET waste alcoholysis with biobased diols and polytransesterification with dimethyl itaconate (DMI), novel poly(diyl itaconate-*co*-terephthalate) copolyesters were synthesized under solvent-free conditions using dibutyltin dilaurate as a catalyst. The resulting polyesters were formulated with reactive diluents and photoinitiators to yield printable resins with up to 22 wt% recycled PET. Mechanical and thermal analysis of 3D printed parts revealed that the incorporation of PET-derived aromatic structures enhanced stiffness, strength, and thermal stability, while the presence of itaconate units enabled high crosslink density and tunable flexibility. The optimal formulation, containing 75 wt% photocurable polyester containing 15.3% recycled PET, achieved a Young's modulus of 1.4 GPa and flexural strength of 54 MPa, representing the highest performance reported to date for itaconic acid-based 3D printable resins. This integrated approach represents a significant green advance by combining solvent-free processing, renewable feedstocks, and post-consumer PET valorisation. The sustainability of the materials was further validated using the Sustainable Formulation Score (SFS), placing the top-performing resins in the top 10% of benchmarked systems.

Received 29th May 2025,
Accepted 15th September 2025

DOI: 10.1039/d5gc02696b

rsc.li/greenchem

Open Access Article. Published on 18 September 2025. Downloaded on 6/28/2026 11:49:16 AM.
This article is licensed under a Creative Commons Attribution-NonCommercial 3.0 Unported Licence.

Green foundation

1. This work establishes a solvent-free, one-pot strategy for converting PET waste and biobased monomers into photocurable polyesters for 3D printing. It integrates chemical recycling with sustainable formulation, enabling resource-efficient, high-value manufacturing through additive techniques with minimal waste.
2. The process incorporates up to 22 wt% recycled PET and achieves 83.1 wt% total sustainable content. Ethylene glycol released from PET depolymerization is reintegrated into the formulation, maximizing atom economy. The use of 3D printing adds inherent sustainability by reducing material waste and enabling decentralized, on-demand production.
3. Further greenness could be achieved by lowering the reaction temperature and time, expanding it to different polyester wastes and increasing the recycled polymer content in the final resins. Broadening the applicability to mixed plastic waste streams and streamlining scalability would also enhance the environmental and industrial impacts of this approach.

Introduction

In today's world, marine and oceanic pollution consists of microscopic and macroscopic polymeric materials that can take over a hundred years to decompose in these environments. It is therefore crucial for researchers to lead the way in developing innovative methods to reduce the production, consumption, and dissemination of new plastic materials in the

[a]*Department of Industrial Chemistry "Toso Montanari", University of Bologna, Bologna 40136, Italy*
[b]*Dpto. Ciencia de los Materiales, I. M. y Q. I., IMEYMAT, Facultad de Ciencias, Universidad de Cádiz, Campus Río San Pedro, s/n, 11510 Puerto Real, Cádiz, Spain. E-mail: mirko.maturi@uca.es*
[c]*Interdepartmental Center for Industrial Research on Advanced Applications in Mechanical Engineering and Materials Technology, CIRI-MAM, University of Bologna, Bologna 40136, Italy*

This journal is © The Royal Society of Chemistry 2025

Open Access Article. Published on 18 September 2025. Downloaded on 6/28/2026 11:49:16 AM. This article is licensed under a Creative Commons Attribution-NonCommercial 3.0 Unported Licence.

marine environment.[1–3] Additionally, they must delve into new and imaginative tactics to repurpose plastic waste into raw materials that can be converted into more sustainable and valuable alternatives. This has been traditionally done by mechanically recycling polymeric waste materials, but only 37.6% of the plastic waste was efficiently recycled in Europe in 2020.[4] Currently, the recycling industry is facing numerous challenges regarding the cost and quality of recycled plastic materials. Furthermore, the accessibility and affordability of petroleum-based monomers create hurdles for recycled materials to compete for wider utilization. Nonetheless, polymer scientists are diligently researching novel chemical techniques to transform plastic waste into more valuable and practical resources.[5,6]

Among the various processing and manufacturing techniques adapted for the mechanical recycling of plastics, additive manufacturing (or 3D printing) has recently emerged as a promising technology for reintroducing plastic waste into the market with enhanced added value.[7,8] To date, this approach has primarily focused on reprocessing thermoplastic waste into blends suitable for extrusion-based technologies, such as fused deposition modelling (FDM).[9] However, mechanical recycling is often limited by the presence of additives and contaminants, which hinder both processing and final material performance.[10] The extent of these limitations is highly dependent on the specific polymer involved. For instance, polyolefins are notoriously difficult to chemically recycle due to their lack of reactive functional groups.[11] In contrast, polyesters like poly(ethylene terephthalate) (PET) contain ester linkages that can be cleaved under catalytic conditions,[12] enabling efficient depolymerization into reusable monomers.[13] Despite this, chemical recycling of PET to regenerate virgin PET remains cost-intensive and complex, particularly because it must compete with virgin PET made from petrochemical sources.[14]

Notably, the production of terephthalic acid (TA) is itself a resource- and energy-intensive process. TA is typically synthesized from petroleum-derived *p*-xylene, which is obtained *via* catalytic reforming and then oxidized in liquid-phase acetic acid under elevated temperature (230 °C) and pressure (350 psi) in the presence of cobalt and manganese catalysts.[15,16] This industrial route involves highly flammable solvents, generates CO and CO_2 as by-products, and requires multiple recrystallization and drying steps to yield purified TA. These considerations highlight the environmental and safety burdens associated with virgin TA production, reinforcing the value of alternative strategies that recover and reuse terephthalate units from post-consumer PET waste through milder, greener chemistries.

In this context, PET depolymerization has also been explored as a gateway to new materials with tailored functionality. For example, sustainable poly(butylene adipate-*co*-terephthalate) (PBAT) can be synthesized using terephthalic acid obtained from PET, offering improved biodegradability through the incorporation of aliphatic units.[17] However, its mechanical performance remains inferior to that of PET, limiting its economic feasibility.[18] Additionally, the synthesis of high-performance polymers typically requires precise control over molecular weight and distribution, necessitating independent depolymerization and repolymerization steps.[19]

Itaconic acid has rapidly emerged as a naturally occurring building block for the preparation of (meth)acrylate-free photocurable formulations that find applications in vat photopolymerization (VP), a 3D printing technique that involves the spatially confined photopolymerization of a liquid resin onto a build plate to create solid objects layer-by-layer.[20] Industrially produced by the fermentation of glucose-rich biomasses, itaconic acid is considered the only naturally occurring compound that possesses a photocurable acrylate moiety, but its additional double carboxylic functionality allows for its employment in the preparation of photocurable esters and polyesters.[21] When co-polymerized with biobased diols such as ethylene glycol (EG), 1,4-butanediol (BDO), 1,6-hexanediol (HDO), and 1,12-dodecanediol (DDO) by Lewis-acid catalysed polytransesterification, it allows fully biobased liquid photocurable polyesters to be obtained that can be formulated with an appropriate amount of reactive diluent and a photoinitiating system to produce sustainable liquid resins for applications in VP 3D printing.[22–25] Interestingly enough, the conditions required for the synthesis of such biobased polyesters are compatible with PET depolymerization and repolymerization, thus opening up the possibility of integrating the two approaches.

In this work, we present the development of an optimized one-pot two-step approach for the depolymerization–repolymerization of PET from water bottle waste into photocurable formulations for VP. To minimize the environmental impact of the approach, polymer transformation was performed in bulk without the need for any solvent and supported by the presence of the minimum quantity of the appropriate metal catalyst. The only reaction by-product was ethylene glycol, which could be integrated into the reactive diluent employed for the formulation of 3D printable resins. The synthesized polyesters were formulated with the appropriate reactive diluents, radical initiators, and stabilizers to achieve a set of photocurable resins that could be 3D printed using VP techniques into solid objects. The PET content and the type of diol were optimized to improve the mechanical properties of the 3D printed material, with the aim of maximizing: (i) the amount of PET that could be included in the final formulation, (ii) the range of achievable mechanical properties, to allow for the production of rigid or flexible materials depending on the specific requirements, and (iii) the quality of the printing process in terms of printing resolution and resin stability. A schematic illustration of the concepts of this work is given in Fig. 1.

Importantly, this strategy aligns closely with key principles of Green Chemistry.[26] The one-pot, solvent-free process minimizes energy and material input (Principles 5 and 6), while the use of renewable itaconic acid and biobased diols supports the use of renewable feedstocks (Principle 7). Post-consumer PET is chemically upcycled, contributing to waste prevention (Principle 1) and enhancing atom economy (Principle 2).

Open Access Article. Published on 18 September 2025. Downloaded on 6/28/2026 11:49:16 AM.
This article is licensed under a Creative Commons Attribution-NonCommercial 3.0 Unported Licence.

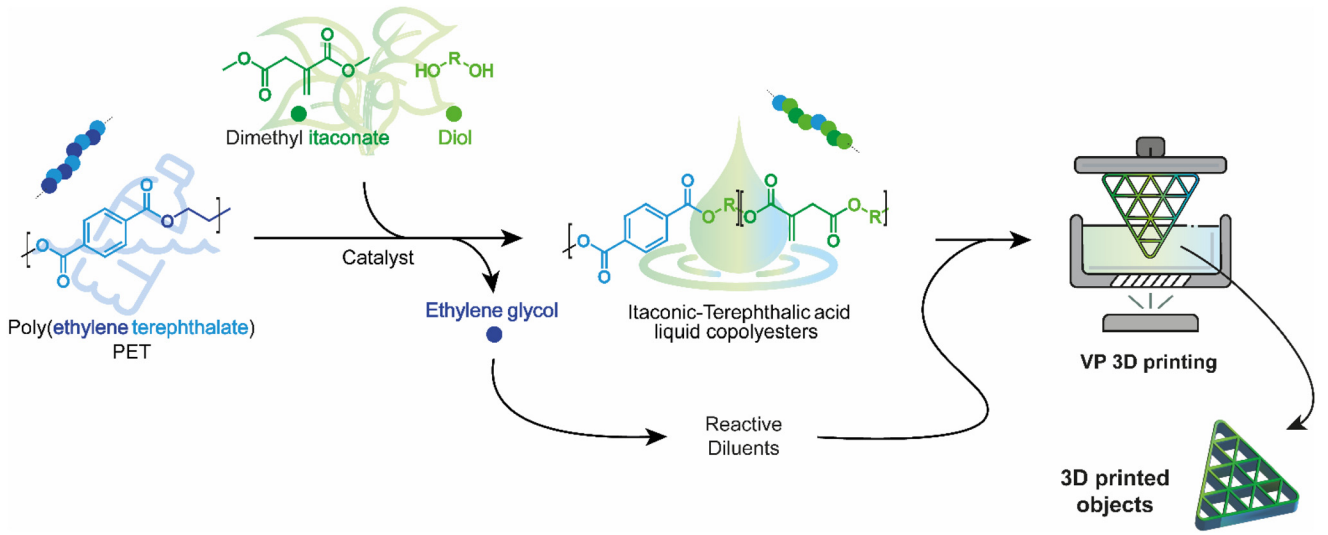

Fig. 1 Complete schematic flowchart of this study. Post-consumer PET is depolymerised, losing the EG that has been recycled into the reactive diluents. Thus, it copolymerises with DMI and diol to form a series of new photopolymerizable vat copolyesters.

Furthermore, the resulting high-performance materials are designed for additive manufacturing, a digital production technique that inherently reduces waste and enables energy-efficient fabrication (Principle 8). Our approach recovers terephthalate units directly from post-consumer PET *via* a mild, solvent-free alcoholysis, eliminating hazardous solvents and reducing energy input while valorizing waste. This offers a significantly greener alternative by closing the loop on aromatic monomer sourcing and avoiding *de novo* petrochemical synthesis.

Experimental section

All chemicals were purchased from Sigma Aldrich (St Louis, MO, USA) and used as received. PET waste (rPET) was obtained by grinding bottles of mixed source into 1–3 mm sized flakes. Prior to use, the flakes were washed by Soxhlet extraction with acetone and dried at room temperature.

One-pot depolymerization–repolymerization of PET waste into poly(diyl itaconate-*co*-terephthalate) photocurable polyesters

Different polyesters were prepared following the same experimental procedure. Details of the amounts of each monomer employed for the different syntheses, as well as the corresponding polymerization yields, are given in Table 1. In a typical process, rPET flakes and the diol(s) were introduced into a 1 L round-bottomed flask equipped with a magnetic stirrer and maintained under an argon atmosphere, along with dibutyltin(IV) dilaurate (DBTDL) as the catalyst. Alcoholysis of rPET was carried out by vigorous stirring of the mixture at 140 °C for 1–3 hours, depending on the proportions of PET, diols, and catalyst, until no visible traces of insoluble PET remained. Subsequently, a distillation setup was attached to the flask, dimethyl itaconate (DMI) was added, and the mixture was stirred at 140 °C under argon, facilitating methanol removal *via* distillation. After 1 hour, when methanol distillation ceased, a vacuum (10 mmHg) was applied to remove unreacted ethylene glycol, which was collected through the distillation setup. Following an additional hour of reaction time, the molten polyester was cooled to room temperature and dissolved in ethyl acetate. The polymer was purified through repeated precipitation in methanol, followed by redissolution in ethyl acetate, and finally dried under reduced pressure. Polymerization yields were calculated as reported in eqn (1):

$$\text{Yield} = \frac{m_{\text{polymer}} + m_{\text{MeOH}} + m_{\text{EG}}}{m_{\text{PET}} + m_{\text{monomers}}} \cdot 100 \quad (1)$$

where m_{polymer} is the mass of obtained photocurable polyester, m_{MeOH} and m_{EG} are the masses of methanol and ethylene glycol separated by distillation during the synthesis, respectively, m_{PET} is the mass of depolymerized–repolymerized rPET used and m_{monomers} is the sum of the masses of all the other monomers used (dimethyl itaconate, diols and eventually dimethyl adipate).

Synthesis of poly(diyl itaconate-*co*-adipate) polyesters

Polymers without repolymerized rPET were synthesized by modifying previously reported methods. In a typical procedure, dimethyl adipate, the diol(s), and dimethyl itaconate, along with DBTDL, were introduced into a 1 L round-bottomed flask fitted with a large magnetic stirrer and connected to a distillation setup. The reaction was carried out at 140 °C under an inert atmosphere for 1 hour, followed by an additional hour under vacuum (10 mmHg). Purification was conducted using the same procedure as described for the synthesis of poly(diyl itaconate-*co*-terephthalate)s.

This journal is © The Royal Society of Chemistry 2025

Open Access Article. Published on 18 September 2025. Downloaded on 6/28/2026 11:49:16 AM. This article is licensed under a Creative Commons Attribution-NonCommercial 3.0 Unported Licence.

Table 1 Amounts and nature of monomer and catalyst employed for the synthesis of the different photocurable polyesters, and the corresponding polymerization yields. Acronyms: BDO = 1,4-butanediol; HDO = 1,6-hexanediol; DDO = 1,12-dodecanediol; DBTDL = dibutyltin(IV) dilaurate; DMI = dimethyl itaconate; DMA = dimethyl adipate; PBIT = poly(butanediyl itaconate-*co*-terephthalate); PDHIT = poly(hexanediyl-*co*-dodecanediyl itaconate-*co*-terephthalate); PBIA = poly(butanediyl itaconate-*co*-adipate); PDHIA = poly(dodecanediyl-*co*-hexanediyl itaconate-*co*-adipate)

Sample	rPET	BDO	HDO	DDO	DBTDL	DMI	DMA	Yield
PBIT_0.2	0.2 mol	1.2 mol	—	—	0.012 mol	1 mol	—	71%
PBIT_0.5	0.5 mol	1.5 mol	—	—	0.015 mol	1 mol	—	75%
PDHIT_0.2	0.2 mol	—	0.6 mol	0.6 mol	0.012 mol	1 mol	—	70%
PDHIT_0.5	0.5 mol	—	0.75 mol	0.75 mol	0.015 mol	1 mol	—	74%
PBIA_0.2	—	1.2 mol	—	—	0.012 mol	1 mol	0.2 mol	58%
PDHIA_0.2	—	—	0.6 mol	0.6 mol	0.012 mol	1 mol	0.2 mol	56%
PDHIA_0.5	—	—	0.75 mol	0.75 mol	0.015 mol	1 mol	0.5 mol	61%

Resin formulation and 3D printing

Photocurable formulations were prepared by formulating the prepared photocurable polyesters at 25, 50, and 75 wt% with pre-mixed 2-hydroxyethyl methacrylate (HEMA), 1,6-hexanediol diacrylate (HDDA), and ethylene glycol phenyl ether acrylate (EGPEA) in a 10 : 7 : 37 weight ratio. To 100 g of such formulations, 2 g of ethyl phenyl(2,4,6-trimethylbenzoyl) phosphinate were added as the photopolymerization initiator, and 1 g of 4-methoxyphenol was added as the radical stabilizer. Then, the mixture was poured into the vat of the VP printer (Phrozen Sonic Mini 8K) and different objects were manufactured using a 405 nm LCD-LED screen with an *XY* resolution of 22 μm and a layer height of 50 μm. Computer-assisted design (CAD) files of 1BA tensile testing specimens according to ISO 527, bending testing specimens according to ISO 178 and complex structures were loaded using the Chitubox v1.9.5 software. The 3D-models were converted into a GCODE file, suitable for 3D-printing. The printed objects were then separated from the printer platform and washed with a 1 : 1 isopropyl alcohol/acetone mixture. Post-processing of the samples was carried out for 60 min in a chamber equipped with a 405 nm light source and a power of 1.25 mW cm^{-2} (FormCure, Formlabs), previously heated to 60 °C.

Green metrics

The rPET content of the photocurable formulation was calculated according to eqn (2):

$$\mathrm{rPET}_{\%} = \mathrm{TA}_{\%} \cdot \mathrm{PP}_{\%} \cdot \frac{\mathrm{MW}_{\mathrm{PET}}}{\mathrm{MW}_{\mathrm{T}}} \quad (2)$$

where $\mathrm{TA}_{\%}$ is the terephthalic acid weight content in the photocurable polyester calculated from NMR data, $\mathrm{PP}_{\%}$ is its concentration, $\mathrm{MW}_{\mathrm{PET}}$ is the molecular weight of the PET monomeric unit (192 g mol^{-1}) and MW_{T} is the molecular weight of the terephthalic acid monomer unit (148 g mol^{-1}).

The biobased carbon content was calculated according to eqn (3). For a formulation containing components i = 1–n, each with its own weight fraction w_i:

$$\mathrm{BCC}_{\%} = \frac{\text{Total biobased carbon mass}}{\text{Total carbon mass}} = \frac{\sum_{i=1}^{n} w_i \mathrm{C}_{\%,i} \frac{n_{\mathrm{BC},i}}{n_{\mathrm{C},i}}}{\sum_{i=1}^{n} w_i \mathrm{C}_{\%,i}} \quad (3)$$

where $\mathrm{C}_{\%,i}$ is the total carbon content of each component i, $n_{\mathrm{BC},i}$ is the number of biobased carbon atoms in its molecular structure and $n_{\mathrm{C},i}$ is the total number of carbon atoms in the molecules of component i.

Finally, the Sustainable Formulation Score (SFS) was calculated for each formulation according to its definition (eqn (4)).[27]

For a formulation containing components i = 1–n, each with its own weight fraction w_i:

$$\mathrm{SFS} = 100 \cdot F_{\mathrm{EoL}} \cdot \sum_{i=1}^{n} (w_i \cdot \mathrm{BCC}_i \cdot F_{\mathrm{syn},i}) \quad (4)$$

where F_{EoL} is defined as the end-of-life factor, and $\sum_{i=1}^{n} (w_i \cdot \mathrm{BCC}_i \cdot F_{\mathrm{syn},i})$ is the weighted sum of the synthetic factors F_{syn} of each component multiplied by the corresponding biobased carbon content, calculated for each component according to eqn (3).

Physical–chemical characterization

^{1}H-NMR spectra were obtained at 298 K on a Bruker (14.01 T, 600.13 MHz) NMR spectrometer. In all recorded spectra, chemical shifts are reported in ppm of frequency relative to the residual solvent signals (^{1}H: 7.26 ppm for $CDCl_3$). ATR-FTIR analyses were performed with a PerkinElmer Spectrum Two spectrophotometer, equipped with a Universal ATR accessory; all spectra were recorded as an average of 20 scans (range 4000–400 cm^{-1} with a resolution of 0.5 cm^{-1}). Rotational viscosity measurements were performed on an Anton Paar MCR102 modular compact rheometer with a CP50-1 geometry, indicating a place-cone geometry with an angle of 1° and a diameter of 25 mm, and rotational frequency ranging from 0.1 Hz to 100 Hz at 25 °C. The effect of temperature on the rotational viscosity was evaluated at a constant shear rate of 1 Hz.

Size exclusion chromatography (SEC)/gel permeation chromatography (GPC) was performed on a HPLC Lab Flow 2000 apparatus, equipped with an injector Rheodyne 7725i, a Phenomenex Phenogel 5 μ MXL column and a Shodex R1-71 refractive index detector. HPLC grade tetrahydrofuran (THF) was used as the eluent with a flow rate of 1 mL min^{-1}. The system was calibrated with polystyrene (PS) standards covering a molar mass range from 300 to 30 000 g

Open Access Article. Published on 18 September 2025. Downloaded on 6/28/2026 11:49:16 AM. This article is licensed under a Creative Commons Attribution-NonCommercial 3.0 Unported Licence.

mol^{-1} (Merck). The mechanical properties of the printed composites were measured using a Shimadzu AGS-X universal testing machine. Tensile and bending testing of the specimens were carried out at 1 mm min^{-1}, in agreement with ISO 527 and ISO 178, respectively. Thermogravimetric analysis (TGA) was performed using a Discovery TGA (TA Instruments) under a N_2 atmosphere with a gas flow of 100 mL min^{-1} and a heating rate of 10 °C min^{-1} from 30 °C to 600 °C.

Results and discussion

One-pot depolymerization–repolymerization reaction

The initial phase of this study focused on identifying the optimal conditions for the polytransesterification of rPET using biobased aliphatic diols and dimethyl itaconate in a single synthetic step. To this end, various Lewis-acid catalysts known for efficiently catalysing PET alcoholysis, such as cobalt(II) acetate, zinc stearate, dibutyl tin(IV) oxide, and dibutyl tin(IV) dilaurate, were evaluated at different concentrations in a mixture containing rPET flakes, butanediol (BDO), and dimethyl itaconate (DMI). A summary of the tested approaches and their outcome is provided in Table S1. While PET was partially depolymerized and dissolved in the reaction mixture with all tested catalysts, the process required elevated temperatures (190 °C) and extended reaction times. Tin-based catalysts were found to actively coordinate with the unsaturation of itaconic acid, leading to crosslinked and insoluble polymers, an outcome exacerbated by the prolonged reaction times and the inherent heterogeneity of the system. Cobalt and zinc salts failed in the repolymerization step, leading to soluble oligomers. To address this challenge, the depolymerization–repolymerization process was divided into two distinct steps within the same flask (one-pot approach) using tin-based catalysts. In the first step, rPET was treated with the diol and the catalyst at an elevated temperature to facilitate polyester alcoholysis. Once all rPET was fully converted, dimethyl itaconate was introduced to initiate the second step, the repolymerization process. By separating the depolymerization and repolymerization stages, the contact time between dimethyl itaconate and the Lewis acid catalyst was minimized, effectively preventing undesired crosslinking reactions. Dibutyl tin(IV) dilaurate (DBTDL) was selected as the optimal catalyst due to its superior activity in polytransesterification, enabling efficient reactions at temperatures as low as 140 °C. In contrast, dibutyl tin oxide (DBTO) required higher temperatures (above 150–160 °C) as it is typically employed at 180–190 °C.[28] In the optimized one-pot, two-step approach, the catalyst activated the ester linkages on the surface of rPET flakes, facilitating their attack by the diol and resulting in a progressive reduction of PET's molecular weight. Ethylene glycol (EG) was generated as a byproduct of PET depolymerization and further participated in the reaction by attacking polyester chains, thereby sustaining the reaction rate.

Compared to conventional chemical recycling of PET *via* glycolysis[29,30] and methanolysis[31,32] (typically 180–220 °C with metal salts), or virgin polyester synthesis *via* melt polycondensation (≥250 °C under vacuum),[33] this method represents a milder alternative in terms of energy input and reaction conditions. The use of DBTDL, a known toxic organotin catalyst, is limited to low concentrations (1 mol%) and ensures high catalytic efficiency at reduced temperatures. After synthesis, the crude polyesters were dissolved in an organic solvent and precipitated in methanol, a standard purification step commonly employed in polyester chemistry to reduce the amount of residual catalyst and low-molecular-weight byproducts.[34–36] While we did not quantify the tin content post-purification, no inhibition of photopolymerization or degradation of mechanical performance was observed in the cured materials, suggesting that any residual catalyst is either effectively removed or immobilized within the crosslinked matrix. Future work will focus on identifying and optimizing greener catalytic alternatives, such as bismuth- or zinc-based systems, which are more compatible with sustainable polymer synthesis while maintaining activity in the presence of unsaturated itaconate moieties.

During the DBTDL-catalysed transesterification, which proceeded to chemical equilibrium, the depolymerization step produced a mixture of terephthalic acid diesters with aliphatic diols, BDO or EG, depending on their relative proportions in the reaction mixture. The molar amount of BDO added was carefully adjusted to equal the combined moles of terephthalic and itaconic acids, as an excess of hydroxyl or acid groups would hinder molecular weight growth in the targeted polyester. The second step followed a mechanism similar to previously reported polytransesterifications involving dimethyl itaconate (DMI) to produce photocurable liquid polyesters.[37] At the elevated reaction temperatures, methanol formed *via* transesterification of DMI evaporated from the solution and was efficiently separated by atmospheric distillation. However, the presence of EG disrupted the molar balance between carboxylic and hydroxyl groups in the reaction mixture, limiting molecular weight growth. To address this issue, once all methanol was removed, the system pressure was reduced to approximately 10 mmHg, lowering EG's boiling point from 197 °C to around 75 °C and enabling its effective removal by distillation. This removal allowed the reaction to drive molecular weight increase in the photocurable polyester, evidenced by a significant increase in the melt viscosity. A schematic representation of the experimental setup is shown in Fig. S1.

Following this approach, several poly(diyl itaconate-*co*-terephthalate)s were prepared, according to the monomer quantities reported in Table 1, which differed by the molar ratio between PET and itaconic acid and by the employed aliphatic diol. When targeting products with terephthalic-to-itaconic molar ratios (N_T/N_I) higher than 0.5, the amount of diol present during the first step appeared to be not enough to allow for PET's efficient depolymerization, significantly increasing the time required for its solubilization. Moreover, due to the increased π-stacking interactions in the photocur-

 This journal is © The Royal Society of Chemistry 2025

Open Access Article. Published on 18 September 2025. Downloaded on 6/28/2026 11:49:16 AM.
This article is licensed under a Creative Commons Attribution-NonCommercial 3.0 Unported Licence.

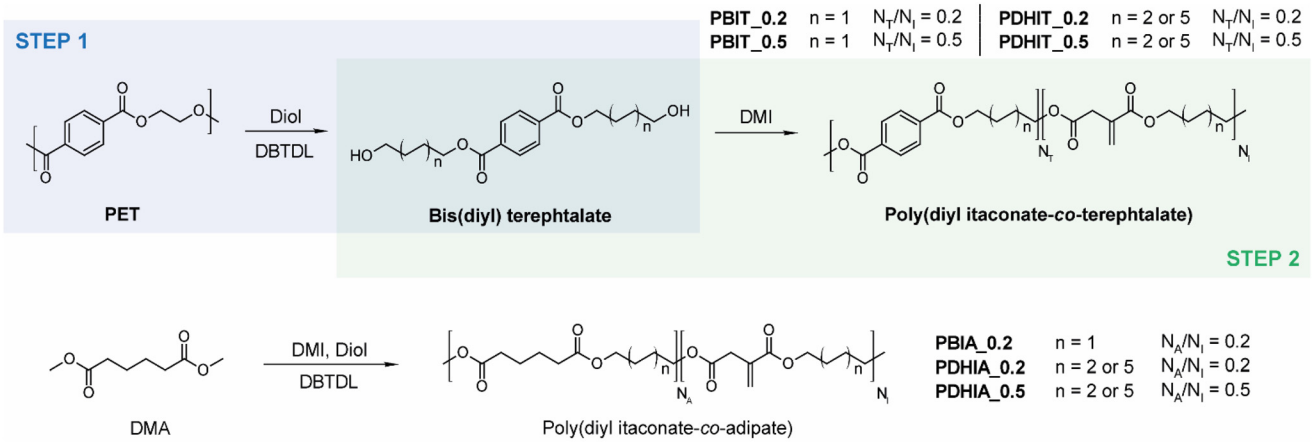

Fig. 2 Synthesis of PET-derived sustainable photocurable polyesters and the corresponding controls prepared with dimethyl adipate (DMA). When BDO was employed as the diol, *n* = 1. When a mixture of HDO and DDO was employed, *n* is statistically either 2 or 5 in equal proportions.

able polyester and the rigidity of the aromatic block, the products obtained in these conditions were solid at room temperature and insoluble in acrylate mixtures, hindering the possibility of their employment in VP processes. Therefore, N_T/N_I values employed in the different syntheses were limited to 0.2 and 0.5, leading to the obtainment of poly(butanediyl itaconate-*co*-terephthalate)s named PBIT_0.2 and PBIT_0.5. The effect of diol chain length on polyester properties, and consequently on 3D-printed materials, was also assessed by substituting BDO with an equimolar mixture of 1,6-hexanediol (HDO) and 1,12-dodecanediol (DDO), thus producing poly(dodecanediyl-*co*-hexanediyl itaconate-*co*-terephthalate)s named PDHIT_0.2 and PDHIT_0.5. Finally, to evaluate the effect of including aromatic monomers in the polyester structure, similar polyesters were prepared replacing terephthalic groups with adipic acid, following previously reported procedures optimized for the use of DBTDL as the catalyst. This led to the preparation of poly(butanediyl itaconate-*co*-adipate), named PBIA_0.2, and poly(dodecanediyl-*co*-hexanediyl itaconate-*co*-adipate)s, named PDHIA_0.2 and PDHIA_0.5. A schematic overview of the synthesized polymers, their structures, and nomenclature is shown in Fig. 2.

Characterization of photocurable polyesters

The prepared photocurable polyesters were firstly characterized by means of ^{1}H-NMR spectroscopy (Fig. S2–S4). The analysis confirmed the effective incorporation of PET-derived terephthalic acid into the poly(itaconate) chains, evidenced by the characteristic aromatic peak at 8.10 ppm. The success of the transesterification reaction was further validated by the absence of signals corresponding to EG units and by the distinct separation between the signals of the alcoholic CH_2 groups of butanediol esterified by itaconic acid (4.05–4.25 ppm) or terephthalic acid (4.31–4.45 ppm). Additionally, by integrating the characteristic NMR signals for each monomer, the actual proportions of the different monomers in the polyesters were determined (Table S2). The results revealed that, in all cases, the amount of terephthalic acid incorporated into the photocurable polyester was 1.4–1.6 times higher than expected from the terephthalate-to-itaconate molar ratios. This discrepancy is likely due to the lower solubility in methanol of terephthalic acid polyesters compared to itaconic acid ones, which led to the partial removal of itaconic acid-rich macromolecules during the purification step.[38,39] This hypothesis is further supported by observations from experiments using dimethyl adipate (DMA) instead of PET. Unlike terephthalic acid, adipate esters have similar solubility to itaconic acid esters, suggesting comparable losses during purification. As a result, the molar ratio between the two diesters in the reaction mixture remained more stable. This effect was also reflected in the polymerization yields (Table 1), which were significantly higher when PET was included in the reaction mixture. Based on the calculated molar ratios of the monomers, the terephthalic acid content in the polyesters ($TA_{\%}$) was found to range from 13.7 wt% to 30.2 wt%. The prepared polymers were further characterized by means of ATR-FTIR spectroscopy, to confirm the predicted macromolecular structure (Fig. 3). As previously reported, the characteristic vibrations of PET macromolecules are the aliphatic C–H bond stretching at 2800–3100 cm^{-1} of the EG unit, the ester carbonyl bond at 1720 cm^{-1}, the aromatic C–H stretching at 1019 cm^{-1}, and the symmetric and asymmetric aromatic C–H bending of the 1,4-disobstituted aromatic ring at 871 cm^{-1} and 731 cm^{-1}.[40,41] The presence of such signals in the spectra of PBITs and PDHITs confirms once again the effective incorporation of terephthalic acid in the photocurable polyester chains, which also showed additional peaks related to the itaconic acid unit such as the weak acrylic C=C stretching band at 1637 cm^{-1} and the vinyl C=C–H bending vibration at 758 cm^{-1}. Analogously, PBIAs and PDHIAs do not present any of the signals related to terephthalic acid units, but they display all the peaks related to aliphatic itaconic acid polyesters, as previously reported.[37]

The molecular weights of the synthesized polyesters were determined using GPC-SEC (Table 2), revealing that all PET-containing polyesters exhibited number-average molecular

Open Access Article. Published on 18 September 2025. Downloaded on 6/28/2026 11:49:16 AM.
This article is licensed under a Creative Commons Attribution-NonCommercial 3.0 Unported Licence.

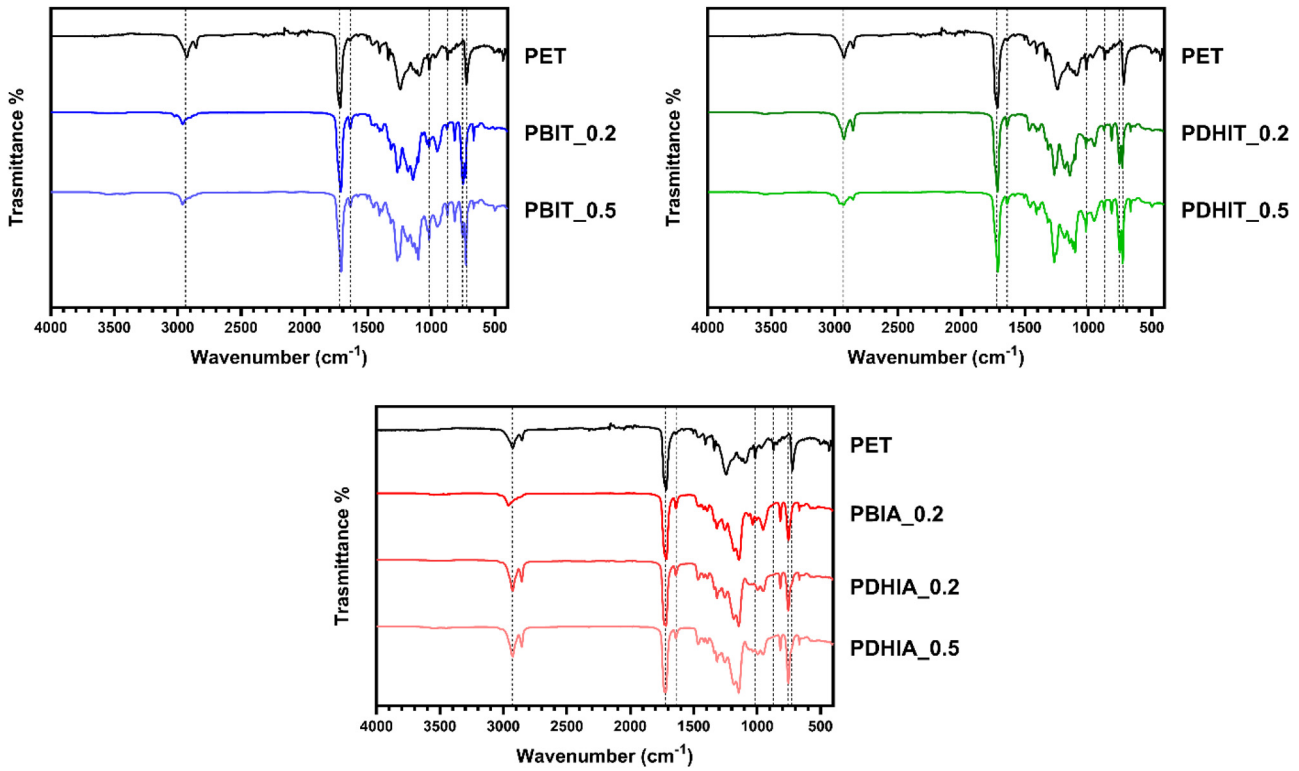

Fig. 3 ATR-FTIR spectra of the starting rPET material and the synthetized photocurable polyesters. Dashed lines correspond in all spectra to wavenumbers (from right to left): 731 cm^{-1}, 758 cm^{-1}, 871 cm^{-1}, 1019 cm^{-1}, 1637 cm^{-1}, 1720 cm^{-1}, and 2931 cm^{-1}.

Table 2 Molecular weight and rotational viscosity (measured at a shear rate of 1 Hz) of the synthetized photocurable polyesters

Sample	$\overline{M_n}$ (kDa)	$\overline{M_w}$ (kDa)	Polydispersity	Viscosity (Pa s)
PBIT_0.2	10.0	29.2	2.9	53
PBIT_0.5	5.3	7.0	1.3	2200
PDHIT_0.2	7.7	10.5	1.4	28
PDHIT_0.5	5.6	7.3	1.3	23
PBIA_0.2	8.1	45.1	5.6	36
PDHAI_0.2	13.2	67.0	5.1	26
PDHAI_0.5	7.4	13.9	1.9	32

weights ($\overline{M_n}$) ranging from 5.3 to 10 kDa. The data indicate that increasing the N_T/N_I ratio from 0.2 to 0.5 resulted in a decrease in the molecular weight across all cases. This reduction is likely due to the higher melt viscosity at elevated N_T/N_I ratios, which hinders the diffusion of the catalyst and reactive species during synthesis. Notably, this effect was significantly less pronounced for PBIA and PDHIA polyesters. Furthermore, the molecular weights measured by GPC align with the integration values of the terminal monomer regions observed in the ^{1}H-NMR spectra, which displayed a consistent trend (Table S2). The high polydispersity indexes observed in the preparations are consistent with previously reported tin-catalysed transesterification methods. This characteristic is advantageous for producing liquid copolyesters with minimal crystallinity, reduced viscosity, and enhanced processability in VP techniques.

The rheological behaviour of the synthetized polyesters was evaluated through their rotational viscosity at different shear rates (Fig. 4), and the values obtained at a frequency of 1 Hz are reported in Table 2. The measured viscosity values reflect a complex interplay between molecular weight and chemical structure. Generally, polymer viscosity increases with molecular weight, as described by the Mark–Houwink equation, due to greater chain entanglement and hydrodynamic volume.[42] However, the data reveal notable deviations from this trend, which can be attributed to structural differences. For instance, polyesters containing longer-chain diols, such as 1,6-hexanediol and 1,12-dodecanediol (PDHIT and PDHIA), exhibit lower viscosities compared to those with only butanediol (PBIT and PBIA), even at comparable or higher molecular weights. This is likely due to increased chain flexibility and reduced intermolecular interactions imparted by the longer aliphatic segments.[43] However, the increasing diol molecular weight necessitates a decrease in dimethyl itaconate content to maintain stoichiometry, especially if accompanied by higher rPET contents, which can compromise photocuring efficiency by lowering the density of unsaturations available for cross-linking, as previously reported.[24] In contrast, increasing the proportion of rigid, aromatic terephthalic acid in PBIT samples leads to a dramatic increase in viscosity, even when

This journal is © The Royal Society of Chemistry 2025

Open Access Article. Published on 18 September 2025. Downloaded on 6/28/2026 11:49:16 AM. This article is licensed under a Creative Commons Attribution-NonCommercial 3.0 Unported Licence.

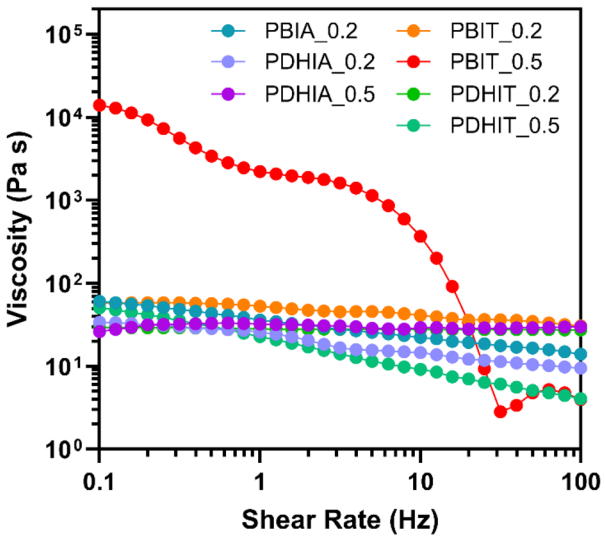

Fig. 4 Rotational viscosity measurement of the synthesized photocurable polyesters at variable shear rates. The measurements were performed at 25 °C.

molecular weight decreases, underscoring the role of backbone rigidity and strong intermolecular interactions in restricting chain mobility.

PBIT_0.5 demonstrates significantly higher viscosity at low shear and the most dramatic shear-thinning behaviour, with the viscosity decreasing by approximately three orders of magnitude as the shear rate increases from 0.1 to 30 Hz, followed by a precipitous drop at higher shear rates that suggests structural breakdown or flow instability. This extreme non-Newtonian behaviour indicates significant entanglement and secondary interactions between polymer chains that are progressively disrupted under increasing shear forces. The PDHIA samples, particularly PDHIA_0.5, display the most Newtonian-like behaviour with relatively stable viscosity across different shear rates, suggesting that the combination of flexible adipic acid units and longer diols creates polymer structures with minimal entanglement and weaker intermolecular interactions. The rPET-based polymers (PBIT and PDHIT) generally show more pronounced shear-thinning than their adipic acid counterparts (PBIA and PDHIA), reinforcing how the rigid aromatic structures influence not only absolute viscosity values but also the nature of flow behaviour under applied stress.

Resin formulation

The synthesized polyesters were incorporated into photocurable formulations for VP at concentrations of 0 wt%, 25 wt%, 50 wt%, and 75 wt%. These formulations used a reactive diluent mixture comprising 2-hydroxyethyl methacrylate (HEMA), 1,6-hexanediol diacrylate (HDDA), and ethylene glycol phenyl ether acrylate (EGPEA) in a 10 : 7 : 37 weight ratio. HEMA and EGPEA were chosen due to their derivation from ethylene glycol, which could potentially originate from the same EG initially bound to terephthalic acid in the original PET macromolecules, thereby increasing the nominal recycled content in the resins. In fact, HEMA is usually produced by monoacylation of EG using methacrylic acid or methyl methacrylate,[44–46] while EGPEA can be prepared by the acrylation of 2-phenoxyethanol, obtained by reacting EG with phenol, cyclohexanone, or cyclohexenone.[47–49] HDDA was included as a partially biobased, low-molecular-weight crosslinker, used in low concentrations to enhance the crosslinking efficiency. To complete the formulation, 2 wt% ethyl phenyl (2,4,6-trimethylbenzoyl)phosphinate was added as a photoinitiator, and 1 wt% 4-methoxyphenol was included as a radical stabilizer. All polymers were easily miscible with the mixture of reactive diluents, leading to liquid resins that possessed rheological properties compatible with the 3D printing process (Fig. S5). Details of the composition, viscosity and biobased content of each formulation are reported in Table 3.

As expected, thanks to the use of low-viscosity reactive diluents, all mixtures display lower viscosity when the polymer content is decreased (Fig. S5). In most cases, viscosity did not surpass the threshold of 10 Pa s, commonly considered the upper limit for printability in VP.[50,51] This was not the case for formulations containing PBIT_0.5, which resulted in the formation of opaque resins at all concentrations tested, which gelled within a few minutes of resting. Given that PBIT_0.5 contained the highest proportion of terephthalic acid units (30.2 wt%), the observed opacity is likely due to the limited solubility of terephthalic acid-rich domains, stabilized colloidally by polyester segments richer in itaconic acid. Once dissolved, the abundant aromatic units in PBIT_0.5 likely engaged in extensive π-stacking interactions, which hindered the fluidity of the mixture and prevented it from flowing autonomously. This is further confirmed by the rheological analysis of its formulations (Fig. S5), which displayed high viscosity especially at low shear rates.

During the VP process, resin flow beneath the 3D printer's build plate is crucial to ensure a fresh supply of material for photocuring and polymerizing subsequent layers. Resins prepared with PBIT_0.5 lacked sufficient flowability, rendering them unsuitable for VP processes and leading to their exclusion from further experiments. In contrast, this issue was not observed for PDHIT_0.5, which contained similar molar content of terephthalic acid, but lower weight content ($TA_{\%}$ = 22.6 wt%) due to the higher molecular weight of the employed diols. This suggests that the maximum permissible terephthalic acid content for producing liquid resins suitable for VP using the presented approach lies near 25 wt%.

Shelf-life monitoring over 12 months at +4 °C in the dark showed no phase separation, gelation, or viscosity drift for optimized resins even in the presence of the photoinitiator. The incorporation of 1 wt% 4-methoxyphenol proved effective in preventing premature polymerization, as previously reported.[22,23]

Sustainability of photocurable formulations

To evaluate the sustainability of each formulation, the overall recycled PET content ($rPET_{\%}$) was calculated from NMR data

Open Access Article. Published on 18 September 2025. Downloaded on 6/28/2026 11:49:16 AM.
This article is licensed under a Creative Commons Attribution-NonCommercial 3.0 Unported Licence.

Table 3 Composition and rotational viscosity (measured at shear rate of 1 Hz) of the prepared photocurable formulations, together with their green metrics. $PP_{\%}$, $HEMA_{\%}$, $HDDA_{\%}$, and $EGPEA_{\%}$ are the weight contents of photocurable polyesters, HEMA, HDDA and EGPEA in each formulation, respectively. Percentages sum up to 97 wt% as the remaining 3 wt% is represented by the photoinitiator and the radical stabilizer. Based on the calculated SFS values and according to its definition, the sustainability of each formulation was ranked with a colour-scale (red = poor, orange = low, yellow = moderate, green = good)

Polyester	$PP_{\%}$	$HEMA_{\%}$	$EGPEA_{\%}$	$HDDA_{\%}$	Viscosity at 25 °C (Pa s)	$rPET_{\%}$	$BCC_{\%}$	SFS	
—	—	18%	66%	13%	0.016	—	23.9%	7.4	
PBIT_0.2	25%	13%	50%	9%	0.031	5.1%	37.2%	20.0	
	50%	9%	32%	6%	0.48	10.2%	51.5%	32.6	
	75%	4%	15%	3%	5.3	15.3%	66.3%	45.2	
PDHIT_0.2	25%	13%	50%	9%	0.041	4.4%	39.5%	19.3	
	50%	9%	32%	6%	0.35	8.9%	55.4%	31.2	
	75%	4%	15%	3%	2.4	13.3%	70.9%	43.1	
PDHIT_0.5	25%	13%	50%	9%	0.049	7.3%	37.5%	19.7	
	50%	9%	32%	6%	0.57	14.7%	51.3%	32.2	
	75%	4%	15%	3%	2.9	22.0%	64.7%	44.6	
PBIA_0.2	25%	13%	50%	9%	0.12	—	41.0%	20.5	
	50%	9%	32%	6%	0.72	—	59.4%	33.6	
	75%	4%	15%	3%	4.2	—	78.7%	46.7	
PDHIA_0.2	25%	13%	50%	9%	0.16	—	42.6%	20.2	
	50%	9%	32%	6%	1.26	—	61.7%	33.0	
	75%	4%	15%	3%	8.8	—	80.5%	45.8	
PDHIA_0.5	25%	13%	50%	9%	0.21	—	42.6%	20.3	
	50%	9%	32%	6%	0.76	—	61.7%	33.4	
	75%	4%	15%	3%	4.0	—	80.5%	46.4	

using eqn (2) for each formulation. In parallel, the biobased carbon content ($BCC_{\%}$) was determined for each formulation based on eqn (3). This parameter reflects the fraction of carbon atoms that potentially originate from biomass-derived or renewable feedstocks, providing a more accurate representation of the formulation's renewable carbon input. Finally, to enable a semi-quantitative assessment of the sustainability of the resins presented in this work, and to allow comparison with previously reported systems, we evaluated them in the Sustainable Formulation Score (SFS) framework.[27] The SFS is a recently introduced green chemistry metric designed to assess the overall sustainability of photocurable formulations for VP, and it has been used to describe around 160 formulations from a sustainability perspective. Unlike traditional metrics, it considers not only the composition and bio-based content of the resin components but also the environmental impact of the synthetic steps required to produce them. Specifically, the SFS integrates parameters such as the hazard profile of the chemicals used, the presence and nature of solvents, reaction temperature and duration, and atom economy (eqn (4)). The values of the calculated green metrics are reported in Table 3.

The first result is the high rPET content achieved in the resin formulations, with a maximum of 22 wt% rPET in the system containing 75 wt% of PDHIT_0.2, followed by 15.3 wt% in the formulation based on 75 wt% PBIT_0.5. While these values may seem modest when compared to other additive manufacturing technologies, such as material extrusion, where rPET can be directly reprocessed at up to 100 wt% without requiring chemical modification, such comparisons do not fully capture the added value of our approach. In vat photopolymerization (VP), the transformation of rPET into photocurable, high-performance formulations enables access to entirely new material properties and application spaces, particularly for functional or high-resolution printed components. Therefore, a direct comparison based solely on rPET content is not appropriate. Nonetheless, to the best of our knowledge, the rPET contents reported here are the highest ever achieved in photocurable formulations designed for VP.

Regarding the biobased carbon content, since PET is not considered as strictly "biobased" according to the definition of $BCC_{\%}$, rPET-containing formulations display lower biobased masses, still widely surpassing 50%. However, this difference becomes negligible when the SFS is calculated, which accounts for the use of waste as a starting material. Hence, in terms of the SFS, the sustainability of the formulations is strongly driven by the presence of itaconic acid-based polyesters, which contribute significantly thanks to their high biobased carbon content and favourable synthetic parameters. The formulations containing 75 wt% these polyesters achieved SFS values that place them in the top 10% of reported systems, above the average value for other itaconic acid-based resins. The values assigned for each synthetic subfactor for the calculation of the SFSs are provided in Table S3.

In addition, although a full life cycle assessment (LCA) of the process is beyond the scope of the current study, existing LCA data on PET chemical recycling and itaconic acid-based systems suggest meaningful reductions in the environmental burden compared to fossil-derived virgin resins.[52–54] For example, the use of itaconic acid derived from glucose-rich biomass has been associated with a 40–60% reduction in greenhouse gas emissions relative to petrochemical analogues. Moreover, solvent-free bulk polymerization and the integration

 This journal is © The Royal Society of Chemistry 2025

Open Access Article. Published on 18 September 2025. Downloaded on 6/28/2026 11:49:16 AM. This article is licensed under a Creative Commons Attribution-NonCommercial 3.0 Unported Licence.

of recovered ethylene glycol directly into the formulation can reduce the number of processing steps and increase atom economy (Green Chemistry Principles 2 and 6).

Mechanical and thermal properties of 3D printed materials

The photocurable formulations were then 3D printed using a commercial VP 3D printer, leading to the obtainment of 3D objects with high resolution and fine details (Fig. 5 and Fig. S6). The higher viscosities of mixtures prepared with 75 wt% photocurable polyester required an adjustment in the build plate's movement speed between layers to allow sufficient time for the resin to flow beneath it. While this modification increased the total printing time by approximately 30%, it did not affect the overall irradiation time, and therefore the total energy consumption, of the 3D printing process.

Then, the photocurable resins were employed to 3D print tensile and flexural test specimens, according to the ISO 527 1BA and ISO 178 specifications, respectively, in order to assess the mechanical properties of the 3D printed materials. The extracted mechanical properties are reported in Fig. 6 and Table S4, while the individual stress–strain plots are available as shown in Fig. S7 and S8. These results allowed for establishing several different correlations between the macromolecular structure of the photocurable polyester and the mechanical properties of the 3D printed materials. By comparing the mechanical properties of all formulations with those of the blank material prepared by polymerizing a mixture of HEMA, EGPEA, and HDDA, it becomes evident that incorporating photocurable polyesters into the formulations caused a progressive decrease in the deformation at break under both tensile and flexural conditions. This effect was often accompanied by an increase in the stiffness and strength. In some instances, particularly with polyesters containing long-chain diols at 25 wt% concentration, the 3D-printed materials exhibited inferior mechanical properties compared to the blank resin. However, when the polyester concentration was raised to 75 wt%, a substantial increase in the Young's modulus and flexural modulus was observed across all cases, frequently alongside improvements in tensile and flexural strengths. As previously reported, the addition of itaconic acid-based polyesters to low-molecular-weight acrylate mixtures induces extensive crosslinking during 3D printing, resulting in the observed reduction in deformability. Nevertheless, in most instances, the pre-formed polyester linkages incorporated into the photopolymer network during the VP process contributed to the system's mechanical resistance, thereby enhancing its overall performance.

Fig. 5 A honeycomb-patterned hollow tennis ball printed with 75% PDHIA_0.5, thus containing 22 wt% recycled PET. Object diameter is 40 mm.

Furthermore, the use of terephthalic acid derived from rPET yielded notable improvements in most mechanical properties compared to analogously prepared polyesters using adipic acid. This effect became more pronounced as the polyester content in the formulations increased. The improvement can be attributed to the higher content of aromatic monomeric groups at elevated polyester concentrations, which facilitated extensive π-stacking interactions, thereby enhancing the material's mechanical resistance.[55]

When BDO was replaced with HDO and DDO in the polyester chains, the resulting macromolecular structures exhibited differences beyond the variation in diol chain length and the associated increase in molecular flexibility. The replacement also led to a reduction in terephthalic acid content, caused by the significantly higher molecular weight of the long-chain diols. This increased chain flexibility resulted in decreased stiffness and improved deformability across all cases, with the effect being particularly pronounced for polyesters derived from rPET (*e.g.*, PBIT_0.2 *vs.* PDHIT_0.2 in Fig. 6). In these cases, the enhanced flexibility of the polyester chains, combined with a reduced terephthalic acid content, diminished the extent of π-stacking interactions within the system. However, increasing the terephthalic acid content by employing PDHIT_0.5 did not enhance the mechanical properties of the material. Instead, the opposite effect was observed. Increasing the terephthalic acid content requires a reduction of itaconic acid, thereby diminishing the polyester's crosslinking ability and ultimately reducing its mechanical properties. These findings indicate that the best-performing material was not PDHIT_0.5 (the formulation with the highest rPET content) but rather PBIT_0.2, which provided an optimal balance between itaconic and terephthalic acid contents. When formulated at a 75 wt% concentration, PBIT_0.2 achieved a Young's modulus of 1.4 GPa and a flexural strength of 54 MPa, values representing the highest performance ever reported for itaconic acid-based resins with a total sustainable content reaching 83 wt%.

Finally, TGA was conducted on 3D-printed samples containing the highest concentration of photocurable polyesters to

Open Access Article. Published on 18 September 2025. Downloaded on 6/28/2026 11:49:16 AM.
This article is licensed under a Creative Commons Attribution-NonCommercial 3.0 Unported Licence.

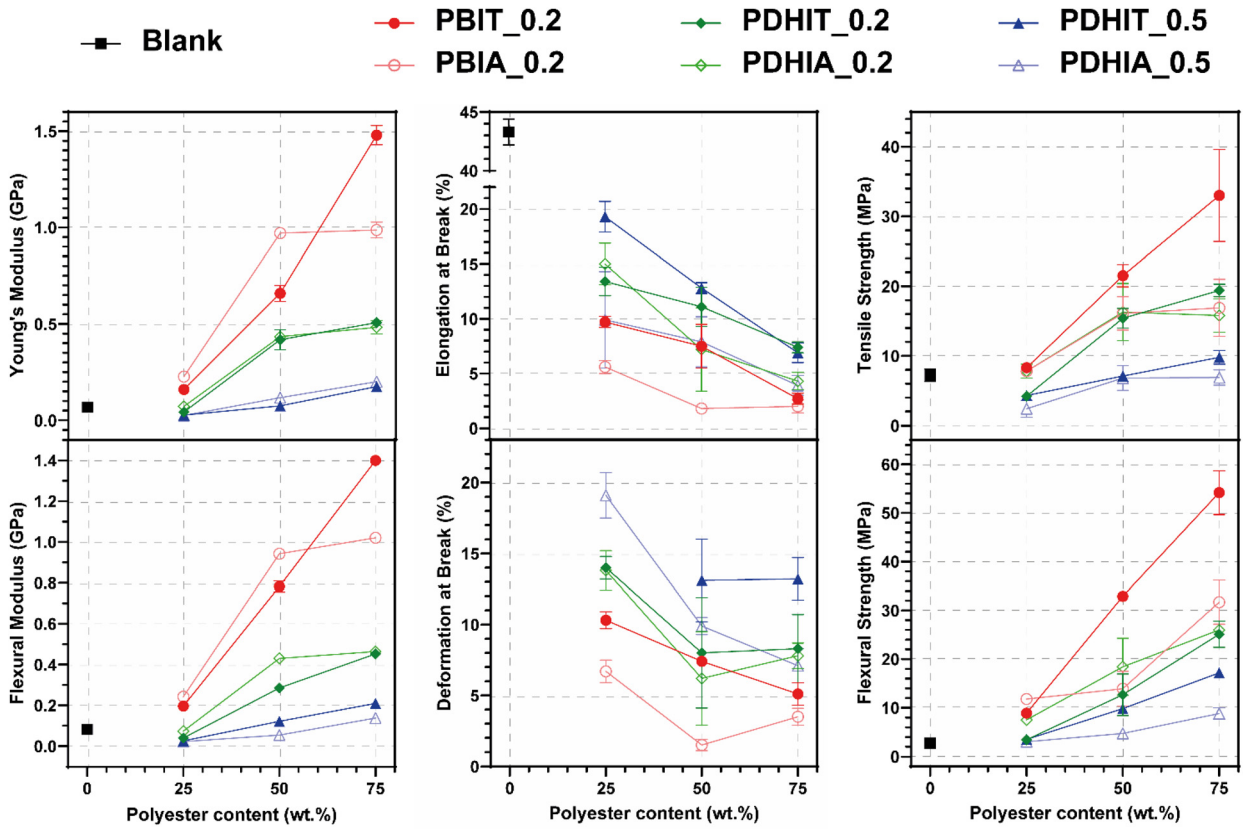

Fig. 6 Tensile and flexural properties of 3D printed materials. Data are expressed as mean ± SD of a set of n = 5 replicates. Deformation at break for resins Blank and PDHIT_0.5 are not reported in the corresponding plot because they did not break during flexural testing.

evaluate the impact of polymer composition on the thermal stability of the printed materials (Fig. S9). The results indicate that the effect of photocurable polyesters on thermal stability varies depending on their macromolecular structure. Specifically, the thermograms reveal that polyesters synthesized with aliphatic diesters (PBIA_0.2, PDHIA_0.2, and PDHIA_0.5) degrade at lower temperatures compared to the blank resin. In contrast, formulations incorporating rPET exhibit enhanced thermal stability relative to the reference resin without photocurable polyesters. This improvement correlates with the terephthalic acid content in each formulation, with higher rPET concentrations leading to greater thermal stability. This trend is further supported by the onset (T_{onset}) and maximum degradation (T_{max}) temperatures reported in Table 4. A plausible explanation for the observed differences in thermal stability is based on the fact that the macromolecular structure of the photocurable polyesters plays a critical role in their degradation behaviour. Crosslinked polyesters synthesized with aliphatic diesters degrade at lower temperatures due to their flexible chains and lower bond dissociation energies, which make them more susceptible to thermal scission. In contrast, rPET-based polyesters incorporate aromatic rings from terephthalic acid that offer enhanced stability through resonance stabilization, increased chain rigidity, and the formation of a protective char during decomposition.[56]

Table 4 Onset and maximum degradation temperatures extracted from TGA analysis of 3D printed materials loaded with 75 wt% different photocurable polyesters

Sample	T_{onset} (°C)	T_{max} (°C)
Blank	359	400
PBIT 0.2	365	410
PDHIT 0.2	360	404
PDHIT 0.5	372	414
PBAI 0.2	353	392
PDHAI 0.2	329	366
PDHAI 0.5	347	385

Replicate batches of photocurable polyesters were synthesized under identical conditions, and printed parts displayed consistent rheological profiles, print quality, mechanical and thermal properties, confirming the reproducibility of the one-pot protocol.

Conclusions

This work presents a solvent-free, one-pot, two-step strategy for the upcycling of post-consumer PET waste into high-performance photocurable polyesters suitable for additive manufacturing *via* vat photopolymerization (VP). The approach

This journal is © The Royal Society of Chemistry 2025

Open Access Article. Published on 18 September 2025. Downloaded on 6/28/2026 11:49:16 AM. This article is licensed under a Creative Commons Attribution-NonCommercial 3.0 Unported Licence.

integrates PET alcoholysis with biobased diols and subsequent polytransesterification with dimethyl itaconate, yielding poly(diyl itaconate-*co*-terephthalate) copolyesters with tunable composition and processability. These were formulated into VP-compatible resins containing up to 22 wt% recycled PET and overall sustainable content reaching 83.1 wt%, ranking among the highest reported for photopolymer systems. Structural tuning of the polyester backbone, achieved by varying the chain length of aliphatic diols, enabled fine control over the resulting polymer's viscosity, mechanical flexibility, and crosslinking density. The presence of rigid aromatic units from recycled terephthalic acid conferred enhanced stiffness and thermal stability, while unsaturated itaconate moieties provided highly reactive vinyl sites for light-activated polymerization. The resulting synergy between molecular architecture and formulation led to a range of printable resins optimized for different mechanical outcomes. In particular, the formulation containing 75 wt% PBIT_0.2 demonstrated a Young's modulus of 1.4 GPa and a flexural strength of 54 MPa, benchmark values for itaconic acid-derived resins and exceeding those for many commercial biobased alternatives. Importantly, this work exemplifies a holistic green chemistry approach by combining waste valorisation, renewable feedstock use, and process intensification. The one-pot design minimizes processing steps and eliminates the need for organic solvents, aligning with principles of energy efficiency, atom economy, and safer synthesis. Furthermore, by incorporating ethylene glycol recovered from PET depolymerization into the reactive diluents, the process closes internal material loops, enhancing circularity within the formulation itself. From a sustainability perspective, the resins were quantitatively evaluated using three metrics: recycled PET content ($rPET_{\%}$), biobased carbon content ($BCC_{\%}$), and the Sustainable Formulation Score (SFS). The best-performing systems ranked within the top 15% of ~160 formulations previously assessed in the SFS framework, validating the environmental relevance of the approach.

The methodology also demonstrates compatibility with industrial VP printing processes, with most formulations exhibiting viscosities within optimal ranges for high-resolution layer-by-layer fabrication. The integration of sustainable chemistry with advanced manufacturing not only reduces environmental burden but also delivers competitive material properties without sacrificing performance. Overall, this study underscores the feasibility of transforming persistent plastic waste into value-added, structurally tunable materials for next-generation applications. It offers a scalable and sustainable route to recyclable, high-performance photopolymers, contributing meaningfully to the development of circular, green manufacturing platforms.

Author contributions

Conceptualization: MM, RC. Data curation: RC. Funding acquisition: MM, SIM, MCF. Investigation: ASdL, RC. Methodology: TB. Supervision: MM, SIM. Writing – original draft: RC, MM. Writing – review and editing: ASdL, MCF, TB, LG, SIM.

Conflicts of interest

There are no conflicts to declare.

Data availability

All data supporting this article are provided within the manuscript and the supplementary information (SI). Supplementary information is available. See DOI: **https://doi.org/10.1039/d5gc02696b**.

Acknowledgements

M. M. acknowledges the Spanish Ministry of Science, Innovation, and Universities for his Juan de la Cierva Formación (FJC2021-047106-I) postdoctoral fellowship. Aroma System S. R. L. is gratefully acknowledged for the financial support provided in the frame of RC's Ph.D. studies (ref. DM 352/2022-M4 C2-Inv. 3.3 Next-GenerationEU). This work was funded by the CEI-MAR (Campus de Excelencia Internacional del Mar) project number CEI-JD-23-05, by the Spanish Ministry of Science, Innovation, and Universities MICIU/AEI/10.13039/501100011033 (Project PID2023-151632OB-C22) and by FEDER, EU. Funding from the University of Cádiz is also acknowledged (research group INNANOMAT, ref. TEP-946).

References

1 M. Bergmann, F. Collard, J. Fabres, G. W. Gabrielsen, J. F. Provencher, C. M. Rochman, E. van Sebille and M. B. Tekman, *Nat. Rev. Earth Environ.*, 2022, **3**(5), 323–337.
2 C. J. Rhodes, *Sci. Prog.*, 2018, **101**, 207–260.
3 M. MacLeod, H. P. H. Arp, M. B. Tekman and A. Jahnke, *Science*, 2021, **373**, 61–65.
4 Eurostat, Recycling rate of plastic packaging waste in the European Union (EU-27) from 2010 to 2020, **https://www.statista.com/statistics/881967/plastic-packaging-waste-recycling-eu/**, (accessed 5 August 2025).
5 S. Kolluru, A. Thakur, D. Tamakuwala, V. V. Kumar, S. Ramakrishna and S. Chandran, *Polym. Bull.*, 2024, **81**, 9569–9610.
6 H. Li, H. A. Aguirre-Villegas, R. D. Allen, X. Bai, C. H. Benson, G. T. Beckham, S. L. Bradshaw, J. L. Brown, R. C. Brown, V. S. Cecon, J. B. Curley, G. W. Curtzwiler, S. Dong, S. Gaddameedi, J. E. García, I. Hermans, M. S. Kim, J. Ma, L. O. Mark, M. Mavrikakis, O. O. Olafasakin, T. A. Osswald, K. G. Papanikolaou, H. Radhakrishnan, M. A. Sanchez Castillo, K. L. Sánchez-Rivera, K. N. Tumu, R. C. Van Lehn, K. L. Vorst,

Open Access Article. Published on 18 September 2025. Downloaded on 6/28/2026 11:49:16 AM. This article is licensed under a Creative Commons Attribution-NonCommercial 3.0 Unported Licence.

M. M. Wright, J. Wu, V. M. Zavala, P. Zhou and G. W. Huber, *Green Chem.*, 2022, **24**, 8899–9002.
7 J. Pakkanen, D. Manfredi, P. Minetola and L. Iuliano, About the Use of Recycled or Biodegradable Filaments for Sustainability of 3D Printing, in *Sustainable Design and Manufacturing 2017*, ed. G. Campana, R. Howlett, R. Setchi and B. Cimatti, SDM 2017, Smart Innovation, Systems and Technologies, Springer, Cham, 2017, vol. 68, DOI: 10.1007/978-3-319-57078-5_73.
8 M. A. Olawumi, B. I. Oladapo, O. M. Ikumapayi and J. O. Akinyoola, *Sci. Total Environ.*, 2023, **905**, 167109.
9 V. Mishra, S. Negi and S. Kar, *J. Mater. Cycles Waste Manage.*, 2023, **25**, 758–784.
10 S. Lodha, B. Song, S. I. Park, H. J. Choi, S. W. Lee, H. W. Park and S. K. Choi, *J. Mech. Sci. Technol.*, 2023, **37**, 5481–5507.
11 L. Zou, R. Xu, H. Wang, Z. Wang, Y. Sun and M. Li, *Natl. Sci. Rev.*, 2023, **10**, nwad207.
12 L. N. Woodard and M. A. Grunlan, *ACS Macro Lett.*, 2018, **7**, 976–982.
13 F. Cao, L. Wang, R. Zheng, L. Guo, Y. Chen and X. Qian, *RSC Adv.*, 2022, **12**, 31564–31576.
14 C. Walberg, The Performance of Recycled Plastics vs Virgin Plastics—Oceanworks, https://oceanworks.co/blogs/ocean-plastic-news/the-performance-of-recycled-vs-virgin-plastics, (accessed 5 August 2025).
15 M. Li, T. Ruddy, D. Fahey, D. H. Busch and B. Subramaniam, *ACS Sustainable Chem. Eng.*, 2014, **2**, 823–835.
16 R. A. F. Tomás, J. C. M. Bordado and J. F. P. Gomes, *Chem. Rev.*, 2013, **113**, 7421–7469.
17 J. Jian, Z. Xiangbin and H. Xianbo, *Adv. Ind. Eng. Polym. Res.*, 2020, **3**, 19–26.
18 W. Thongsong, C. Kulsetthanchalee and P. Threepopnatkul, *Mater. Today: Proc.*, 2017, **4**, 6597–6604.
19 M. Kirstein, C. Lücking, L. Biermann, E. Brepohl, V. Salikov, C. Eichert, M. Paschetag and S. Scholl, *Chem. Ing. Tech.*, 2023, **95**, 1290–1296.
20 S. Pérocheau Arnaud, N. M. Malitowski, K. Meza Casamayor and T. Robert, *ACS Sustainable Chem. Eng.*, 2021, **9**, 17142–17151.
21 S. Pérocheau Arnaud, E. Andreou, L. V. G. Pereira Köster and T. Robert, *ACS Sustainable Chem. Eng.*, 2020, **8**, 1583–1590.
22 C. Spanu, E. Locatelli, L. Sambri, M. Comes Franchini and M. Maturi, *ACS Appl. Polym. Mater.*, 2024, **6**, 2417–2424.
23 R. Carmenini, C. Spanu, E. Locatelli, L. Sambri, M. Comes Franchini and M. Maturi, *Prog. Addit. Manuf.*, 2024, **9**, 2499–2510.
24 M. Maturi, C. Spanu, E. Locatelli, L. Sambri and M. Comes Franchini, *Addit. Manuf.*, 2024, **92**, 104360.
25 M. Maturi, S. Maturi, A. Sanz de León, L. Migliorini, M. de la Mata, T. Benelli, L. Giorgini, P. Milani, M. Comes Franchini and S. I. Molina, *ACS Appl. Polym. Mater.*, 2025, **7**, 4371–4382.
26 S. L. Y. Tang, R. L. Smith and M. Poliakoff, *Green Chem.*, 2005, **7**, 761–762.
27 M. Maturi, E. Locatelli, A. Sanz de León, M. Comes Franchini and S. I. Molina, *Green Chem.*, 2025, **27**, 8710–8754.
28 A. B. Ferreira, A. L. Cardoso and M. J. da Silva, *Int. Scholarly Res. Not.*, 2012, 142857.
29 L. Bartolome, M. Imran, K. G. Lee, A. Sangalang, J. K. Ahn and D. H. Kim, *Green Chem.*, 2013, **16**, 279–286.
30 D. Carta, G. Cao and C. D'Angeli, *Environ. Sci. Pollut. Res.*, 2003, **10**, 390–394.
31 J. Li, D. Yan, X. Cheng, C. Rong, J. Feng, X. Feng, J. Xin, Q. Zhou, Y. Li, J. Xu and X. Lu, *Ind. Eng. Chem. Res.*, 2024, **63**, 12373–12384.
32 D. D. Pham and J. Cho, *Green Chem.*, 2021, **23**, 511–525.
33 K. Pang, R. Kotek and A. Tonelli, *Prog. Polym. Sci.*, 2006, **31**, 1009–1037.
34 B. S. Rajput, T. A. P. Hai, N. R. Gunawan, M. Tessman, N. Neelakantan, G. B. Scofield, J. Brizuela, A. A. Samoylov, M. Modi, J. Shepherd, A. Patel, R. S. Pomeroy, N. Pourahmady, S. P. Mayfield and M. D. Burkart, *J. Appl. Polym. Sci.*, 2022, **139**, e53062.
35 Z. Terzopoulou, E. Karakatsianopoulou, N. Kasmi, V. Tsanaktsis, N. Nikolaidis, M. Kostoglou, G. Z. Papageorgiou, D. A. Lambropoulou and D. N. Bikiaris, *Polym. Chem.*, 2017, **8**, 6895.
36 H. R. Kricheldorf and S. M. Weidner, *Polym. Chem.*, 2022, **13**, 1618–1647.
37 M. Maturi, C. Spanu, E. Maccaferri, E. Locatelli, T. Benelli, L. Mazzocchetti, L. Sambri, L. Giorgini and M. C. Franchini, *ACS Sustainable Chem. Eng.*, 2023, **11**, 17285–17298.
38 F. Stempfle, B. S. Ritter, R. Mülhaupt and S. Mecking, *Green Chem.*, 2014, **16**, 2008–2014.
39 J. Tang, X. Meng, X. Cheng, Q. Zhu, D. Yan, Y. J. Zhang, X. Lu, C. Shi and X. Liu, *Ind. Eng. Chem. Res.*, 2023, **62**, 4917–4927.
40 Z. Chen, J. N. Hay and M. J. Jenkins, *Eur. Polym. J.*, 2012, **48**, 1586–1610.
41 C. Ioakeimidis, K. N. Fotopoulou, H. K. Karapanagioti, M. Geraga, C. Zeri, E. Papathanassiou, F. Galgani and G. Papatheodorou, *Sci. Rep.*, 2016, **6**(1), 1–8.
42 W. L. Hergenrother and C. J. Nelson, *J. Polym. Sci., Polym. Chem. Ed.*, 1974, **12**, 2905–2915.
43 Z. Zeng, L. Sun, W. Xue, N. Yin and W. Zhu, *Polym. Test.*, 2010, **29**, 66–71.
44 J. Li and F. He, CN109134245A, 2019.
45 S. A. Torosyan, Y. N. Biglova, V. V. Mikheev, Z. T. Khalitova, F. A. Gimalova and M. S. Miftakhov, *Mendeleev Commun.*, 2012, **22**, 199–200.
46 M. Macret and G. Hild, *Polymer*, 1982, **23**, 81–90.
47 C. A. Horiuchi, H. Fukunishi, M. Kajita, A. Yamaguchi, H. Kiyomiya and S. Kiji, *Chem. Lett.*, 1991, **20**, 1921–1924.
48 H. Y. Lin and S. A. Dai, *J. Chin. Chem. Soc.*, 2010, **57**, 167–173.
49 M. Sutter, N. Sotto, Y. Raoul, E. Métay and M. Lemaire, *Green Chem.*, 2013, **15**, 347–352.

 This journal is © The Royal Society of Chemistry 2025

Open Access Article. Published on 18 September 2025. Downloaded on 6/28/2026 11:49:16 AM.
This article is licensed under a Creative Commons Attribution-NonCommercial 3.0 Unported Licence.

50 I. A. Timofticiuc, O. Călinescu, A. Iftime, S. Dragosloveanu, A. Caruntu, A. E. Scheau, I. A. Badarau, A. C. Didilescu, C. Caruntu and C. Scheau, *J. Funct. Biomater.*, 2023, **15**, 7.
51 C. Kasprzak, J. R. Brown, K. Feller, P. J. Scott, V. Meenakshisundaram, C. Williams and T. Long, *ACS Appl. Mater. Interfaces*, 2022, **14**, 18965–18973.
52 M. Iturrondobeitia, L. Alonso and E. Lizundia, *Resour., Conserv. Recycl.*, 2023, **198**, 107182.
53 S. Chairat and S. H. Gheewala, *Environ. Res.*, 2023, **236**, 116788.
54 R. Rebolledo-Leiva, M. T. Moreira and S. González-García, *Bioresour. Technol.*, 2022, **345**, 126481.
55 B. Bottega Pergher, D. H. Weinland, R. J. van Putten and G. J. M. Gruter, *RSC Sustainability*, 2024, **2**, 2644–2656.
56 J. D. Menczel and R. Bruce Prime, *Thermal analysis of polymers*, John Wiley, 2009.